Journal of Solid State Chemistry xxx (xxxx) 124889

Contents lists available at ScienceDirect

Journal of Solid State Chemistry

journal homepage: www.elsevier.com/locate/jssc

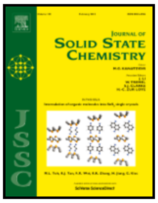

Synthesis, crystal and electronic structures of two novel tunnel bismuth oxychlorides $Bi_{18}O_{22}Cl_{8.5}(BO_3)_{0.5}$ and $Bi_{18}O_{22}Cl_8Se$

Dmitri O. Charkin [a, b], Sergey N. Volkov [b], Alexey N. Kuznetsov [a], Alexey Povolotskiy [c], Anastasia P. Chernyatieva [d], Julia S. Mironova [e], Sergey M. Aksenov [b, f, *]

[a] Department of Chemistry, Moscow State University, Vorobievy Gory 1-3, Moscow, 199991, Russia
[b] Laboratory of Arctic Mineralogy and Material Sciences, Kola Science Centre, Russian Academy of Sciences, Apatity, Russia
[c] Institute of Chemistry, Saint Petersburg State University, St. Petersburg, Russia
[d] Department of Crystallography, Saint Petersburg State University, St. Petersburg, Russia
[e] Department of Materials Sciences, Moscow State University, Vorobievy Gory 1-73, Moscow, 199991, Russia
[f] Geological Institute, Kola Science Centre, Russian Academy of Sciences, Apatity, Russia

CORRECTED PROOF

ARTICLE INFO

Keywords:
Anion-centered tetrahedra
2D zeolites
Bismuth oxychlorides
Tunnel oxides
Anti-Zeolite

ABSTRACT

Single crystals of two new quaternary bismuth oxychlorides, $Bi_{18}O_{22}Cl_{8.5}(BO_3)_{0.5}$ **(1)** and $Bi_{18}O_{22}Cl_8Se$ **(2)**, have been serendipitously produced in syntheses starting from bismuth borate or oxyselenide and oxychloride. The crystal structure of **1** represents a high symmetry analog of the $PbBi_{17}O_{22}Cl_9$ type structure, formed by double aliovalent ($Pb^{2+} \rightarrow Bi^{3+}$, $0.5Cl^- \rightarrow 0.5BO_3^{3-}$) substitution at the two respective cationic and anionic sites, while **2** is a full structural analog of $PbBi_{17}O_{22}Cl_9$. Overall, their structures can be described as sequences of thick (16 Å) slabs (2D "host" structure) comprised of litharge–like layers and ribbons formed by edge-shared oxocentered OBi_n, polyhedra ($n = 4$ and 5). The chloride anions fill the 7.6 Å channels with the triangular cross-section inside the slabs as well as the interlayer space wherein they are partially substituted by disordered BO_3^{3-} groups or Se^{2-} anions. Compound **1** is just the second example of a mixed halide–borate occupancy among bismuth compounds while **2** illustrates much broader perspectives of mixed oxyhalide–oxychalcogenide approach to construction of novel complex bismuth compounds. Both compounds make new contributions to the family of tunnel structures of anion-centered tetrahedra featuring wide trigonal channels filled by halide anions or more complex metal–halide "salt inclusions".

1. Introduction

By now, multinary oxide halides of trivalent bismuth are widely studied due to a variety of practically important properties wherein many representatives of this amazing family exhibit high performance. Ferroelectricity [1,2], nonlinear optical activity [2], catalytic activity in a variety of processes starting from selective oxidation of hydrocarbons to photodegradation of organic waste [3–7], luminescence [8], and thermoelectricity [9] are just the few that initiated extensive explorations spreading in disparate directions. Some of these properties arise already at the level of the corresponding pseudo–binary bismuth oxide – bismuth halide systems of which the oxychlorides have attracted the greatest interest due to higher thermal and air stability. The crystal structures of the overwhelming majority contain either litharge–like layers or their fragments comprised of oxygen–centered OBi_4 tetrahedra and OBi_3 triangles [10,11]. The most commonly referred to are the Sillén–like compounds BiOX or $M^{II}BiO_2X$ (X = Cl, Br, I) [12,13]; yet, many more complex mixed–layer structures have been reported. The commonly addressed way of further development of this family is in increasing the chemical complexity by adding more components. Until recently, this was achieved almost exclusively by introducing various cationic species [14,15]; the last decade also witnesses rapid development of multi–anionic structures [9,16–18].

Many complex bismuth-oxide and lead-fluoride halides or chalcogenides can be characterized by the microporous positively-charged frameworks related to zeolite-like structure, formed by anion-centered $[OBi_n]^{p+}$ or $[OPb_4]^{q+}$ polyhedra [11]. These frameworks are characterized by the presence of wide channels and/or large cavities filled by negatively-charged guest anions. Such inversion between the charges of host structure and the guest is well-known for the compounds belong to the co-called "antizeolite" family [19,20]. In particular, among bismuth compounds such frameworks are present in the crystal structures of

---

* Corresponding author. Laboratory of Arctic Mineralogy and Material Sciences, Kola Science Centre, Russian Academy of Sciences, Apatity, Russia.
E-mail address: aks.crys@gmail.com (S.M. Aksenov).

https://doi.org/10.1016/j.jssc.2024.124889
Received 1 March 2024; Received in revised form 2 July 2024; Accepted 5 July 2024
0022-4596/© 20XX

Note: Low-resolution images were used to create this PDF. The original images will be used in the final composition.

$Bi_4O_3(BO_3)_2$ [21], Bi_5O_7I [22], $Bi_{14}O_{20}(SO_4)$ [23], $Bi_{12}O_{15}Cl_6$ [24], $Bi_6O_7FCl_3$ [25], and $Bi_{48}O_{59}Cl_{30}(M_5Cl)$ (M = Cu^+, Ag^+) [26], while for lead compounds the most complex framework is reported for the crystal structure of $[Pb_{12}F_{16}][Ta_9O_{20}F_{13}]$ [27]. Reduction of dimensionality of the anion-centered host structure with the preservation of the system of parallel channels forming **2D** zeolite-related compounds has been previously found in $PbBi_{17}O_{22}Cl_9$ and $Na_2Bi_{12}O_{15}Cl_8$ [28] wherein wide layers are structurally related to those in $Bi_6O_7FCl_3$ [25] and $Bi_{48}O_{59}Cl_{30}(M_5Cl)$ (M = Cu^+, Ag^+) [26], respectively.

Herein we report synthesis and crystal structures of two new compounds with a more complex "steelwork" architecture, which are the multi–anionic analogs of a multi–cationic archetype. One of these, $Bi_{18}O_{22}(BO_3)_{0.5}Cl_{8.5}$ (**1**), was serendipitously observed as a minor by–product in the search for the chloride analog of a recently reported incommensurately modulated compound Bi_4BO_7Cl [29]. Several crystals of its analog, $Bi_{18}O_{22}SeCl_8$ (**2**), were equally unexpectedly obtained during the preparation of a known compound $Bi_4O_4SeCl_2$ [17]; their multi–cationic archetype is the unique compound $PbBi_{17}O_{22}Cl_9$ [28]. We also discuss crystal chemistry of microporous bismuth "salt–inclusion" structures with the trigonal channels of varied effective width in terms of zeolite-related structures.

2. Experimental

2.1. Synthesis

The crystals of **1** were produced as a minor side product upon synthesis aimed at the preparation of Bi_4BO_7Cl [29]. In the first step, a "Bi_3BO_6" precursor was prepared by slowly heating a mixture of bismuth nitrate pentahydrate (p.a.) and boric acid (extra pure) in 2:3 M ratio in an open alumina crucible to 723 K. The sample was ground and re–heated at 923 K for 48 h. It was then cooled down to room temperature and mixed with BiOCl (prepared by hydrolysis of $BiCl_3$ in excess water) in 1:1 M ratio and annealed in a silica–jacketed alumina crucible at 1123 K for 48 h, after which the furnace was switched off. The major part of the sample was microcrystalline yellow Bi_4BO_7Cl [29]; just a few druses of thin needle–like crystals of **1** were found at the top part of the sample (Fig. 1).

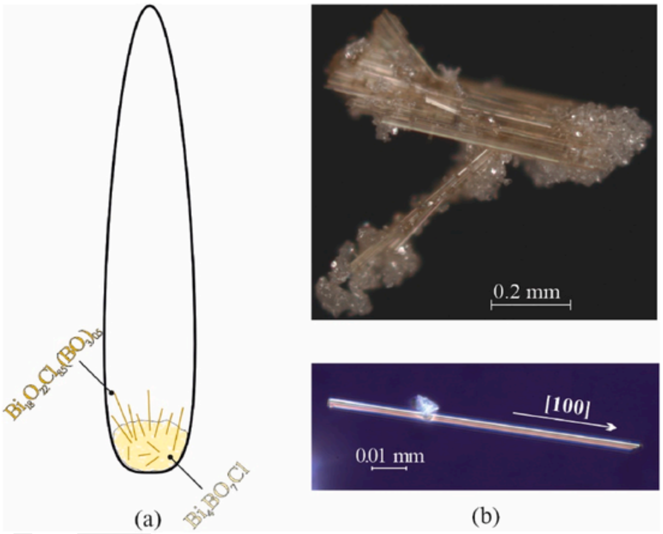

Fig. 1. (a) Schematic diagram of experimental setup for the synthesis of $Bi_{18}O_{22}Cl_{8.5}(BO_3)_{0.5}$. The figure shows an evacuated quartz glass ampoule, at the bottom of which there is a charge of the stoichiometric composition "Bi_4BO_7Cl", from which long and thin needles of $Bi_{18}O_{22}Cl_{8.5}(BO_3)_{0.5}$ protruded. (b) Single crystals of $Bi_{18}O_{22}Cl_{8.5}(BO_3)_{0.5}$ in non-polarized (above) and polarized (below) light.

The crystals of **2** were observed on the surface of a pellet aimed at the preparation of $Bi_4O_4SeCl_2$. BiOCl and Bi_2O_2Se (prepared from Bi (extra pure), Bi_2O_3 (p.a.), and Se (extra pure) at 1023 K as described in Ref. [30]) were taken in 2:1 M ratio, pelletized, and annealed in an evacuated silica ampoule at 1073 K for 60 h. Black needles of the new compound were observed on the upper surface of the pellet along with colorless platelets of BiOCl and off-white isometric crystals of $Bi_4Si_3O_{12}$ [31]. All attempts to substitute, even partially, Cl by Br in **1** or **2** were as yet of no success.

After establishing the composition of the new compounds from single crystal studies (vide infra), attempts were made to prepare bulk samples. For **1**, a stoichiometric mixture of Bi_3BO_6, Bi_2O_3, and BiOCl was annealed under the same conditions as described above. For **2**, a mixture of Bi_2O_3, Bi_2O_2Se, and BiOCl was pressed into a pellet (at *ca.* 8 t/cm^2), sealed into a silica tube and annealed at 1123 K. The target products were dominant, yet single-phase specimens could not be attained (Fig. S1): the samples contained 63 % $Bi_{18}O_{22}Cl_{8.5}(BO_3)_{0.5}$ and 52 % $Bi_{18}O_{22}Cl_8Se$ (with the BiOCl present in both samples as a major common impurity). Powder X–ray diffraction (PXRD) patterns were collected on Rigaku SmartLab SE diffractometer (3 kW sealed X–ray tube, D/teX Ultra 250 silicon strip detector, vertical type θ–θ geometry, HyPix–400 (2D HPAD) detector) utilizing Cu Kα radiation ($\lambda_{K\alpha 1}$ = 1.54060 Å, $\lambda_{K\alpha 2}$ = 1.54433 Å).

2.2. Single–crystal X–ray analysis

A needle–like crystal of **1** was selected using the polarizing microscope and mounted on a glass fiber. The data were collected on a Rigaku XtaLAB Synergy–S four–circle diffractometer utilizing Mo Kα radiation. Lorentz and polarization corrections were applied; the absorption correction was made using multi–scan method. An isotropic extinction–correction did not improve the refinement for all crystals. The intensities of the reflections for the tiny crystal of **2** were collected at the "Belok" beamline of the Kurchatov Synchrotron Radiation Source (NRC "Kurchatov Institute", Moscow, Russia), at the wavelength of 0.7572 Å using a MAR CCD 165 detector. The image integration was performed using the iMosflm software [32]. The integrated intensities were empirically corrected for the absorption using the Scala program [33].

The observed Laue symmetry and systematic absences indicated *Immm* space group for **1** and *C*2/*c* for **2**. The structures were solved using a charge–flipping method [34] implemented in JANA2020 [35]. Data visualization was performed with the Vesta [36] and Atoms 6.1 [37] software.

Initially, 6 Bi, 4 Cl, and 7 O sites were localized for **1** which led to an incomplete formula of «$Bi_{18}O_{22}Cl_8$» with a semi–occupied Cl4 position. Analysis of the difference electron density maps revealed several weak additional maxima around Cl4. Initially, the overall formula was balanced to « $Bi_{18}O_{22.5}Cl_8$» but some interatomic distances were out of conventional ranges. Therefore, we suspected that, by analogy to Bi_4BO_7Cl [29], the structure of **1** contains a mixed–occupied anion site hosting the Cl^- and BO_3^{3-} in a 0.75:0.25 ratio, resulting in a change-balanced $Bi_{18}O_{22}Cl_{8.5}(BO_3)_{0.5}$ formula. Assuming that both Cl^- and the boron atom occupied the same position, the distances to the weak additional maxima matched fairly to two equiprobable positions of a trigonal borate group. Solution and subsequent refinement of **2** revealed 6 Bi, 3 Cl, 7 O positions and one mixed Se/Cl position. The main features of the X–ray diffraction experiments and structure refinement are summarized in Table 1. Final atomic positional and displacement parameters, selected bond lengths and angles are given in Table S1–S6.

The bond–valences sums have been calculated using the Brown–and–Altermatt bond–valence parameters [38] and are listed in

UNCORRECTED PROOF

CORRECTED

Table 1
Experimental details.

Chemical formula	$B_{0.5}Bi_{18}Cl_{8.5}O_{23.5}$	$Bi_{18}Cl_8O_{22}Se$
M_r	4444.4	4476.2
Crystal system, space group	Orthorhombic, *Immm*	Monoclinic, *C*2/*m*
Temperature (K)	296	293
Unit cell parameters	a = 39.4183 (2) Å b = 11.6965 (6) Å c = 3.888 (2) Å	a = 38.888 (8) Å b = 11.6700 (8) Å c = 3.8700 (8) Å β = 95.69 (3) °
V (Å^3)	1792.4 (9)	1747.7 (5)
Z	2	2
Radiation type	Mo *Kα*	Synchrotron, λ = 0.7572 Å
μ (mm^{-1})	88.7	99.90
Crystal size (mm)	0.18 × 0.02 × 0.02	0.11 × 0.12 × 0.16
Data collection		
Diffractometer	XtaLAB Synergy, Single source at home/near, HyPix	Synchrotron, λ = 0.7572 Å
Absorption correction	Based on crystal shape	Based on crystal shape
T_{min}, T_{max}	0.018, 0.333	0.139, 0.645
No. of measured, independent and observed [$I > 3\sigma(I)$] reflections	7191, 1673, 919	15249, 1600, 1598
R_{int}	0.067	0.143
$(\sin \theta/\lambda)_{max}$ (Å^{-1})	0.777	0.682
Refinement		
$R[F^2 > 2\sigma(F^2)]$, $wR(F^2)$, S	0.059, 0.048, 1.66	0.055, 0.065, 1.99
No. of reflections	1673	1600
No. of parameters	74	91
$\Delta\rho_{max}$, $\Delta\rho_{min}$ (e Å^{-3})	3.11, −3.95	3.29, −3.08

Computer programs: *CrysAlis PRO* 1.171.41.93a (Rigaku OD, 2020).

Tables S1 and S2. All bond valence sums are in good agreement with the expected formal valences of atoms in the structure. In order to get more insights into the possible pathways for sodium diffusion, the Bond Valence Energy Landscape (BVEL) was calculated using to the Bondstr software [39] provided in the Fullprof suite [40].

2.3. EDX analysis

Energy–dispersive X–ray spectroscopy (EDX) of **1** was performed on a Zeiss EVO–25 scanning electron microscope (SEM) equipped with an Oxford Instruments Ultum–Max 100 Energy Dispersive Spectrometer. The electron–beam accelerating voltage was 20 kV and the current 2 nA; defocused beam (up to 4 μm spot size) was used and the X–ray acquisition time was 100 s. The chemical composition was measured on different spots on several crystals and eventually averaged. EDX analysis of **1** yielded Bi:O:Cl molar ratios of approximately 17.3:26.0:6.7 for **1**, which is close to the expected 18.0:23.5:8.5, considering the considerable overlapping of the analytical Bi*M* and Cl*K* lines (Fig. S2).

2.4. Rietveld analysis

The Rietveld refinement was performed on the powder diffraction pattern of **1** and **2**. Sample of **1** consisted of individual crystals, selected from a sample obtained during the synthesis of Bi_4BO_7Cl. 10–15 single crystals of 0.1–0.2 mm size were selected in an optical microscope, ground under ethanol and transferred, as a suspension, onto a low–background single–crystalline germanium holder. The sample of **2** was in amount sufficient for the use of glass holder. The final structure models of **1** and **2** obtained from single–crystal data were used in the refinement utilizing RietveldToTensor software [41]. Pseudo–Voigt functions were used for fitting the reflection profiles. The background was described by a Chebyshev polynomial function (25th order) and the preferred orientation (direction [001] for **1** and [100] for **2**) was modeled by the March–Dollase approach. The atomic coordinates were not refined. The final Rietveld refinement results are given in Fig. 2 and Table 2. The final refinement resulted in R_{wp} = 0.058 and R_B = 0.068. The results obtained from the powder diffraction data are in proper agreement with those derived from the single–crystal data.

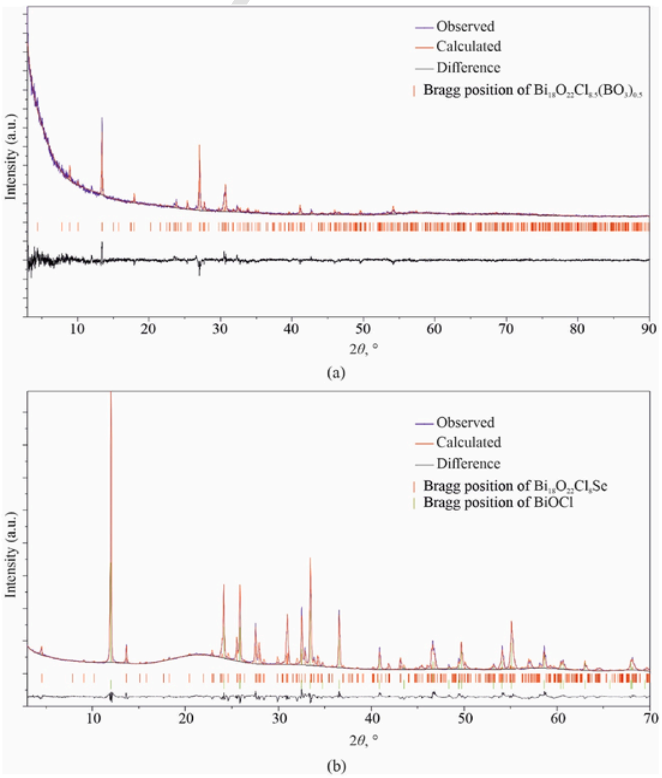

Fig. 2. Intensity profiles for the powder X–ray Rietveld refinement of (a) $Bi_{18}O_{22}Cl_{8.5}(BO_3)_{0.5}$ and (b) $Bi_{18}O_{22}Cl_8Se$. The observed and calculated profiles are represented in blue and red lines, respectively. The difference profile is plotted at the bottom. Vertical bars indicate the positions of the Bragg reflections.

Table 2
X–ray Rietveld refinement of the $Bi_{18}O_{22}Cl_{8.5}(BO_3)_{0.5}$ structure.

Chemical formula	$Bi_{18}O_{22}Cl_{8.5}(BO_3)_{0.5}$	$Bi_{18}O_{22}Cl_8Se$
M_r	4444.4	4476.2
Temperature (K)	297	297
Crystal system, space group	Orthorhombic, *Immm*	Monoclinic, *C*2/*m*
Unit–cell parameters	a = 8.88622 (27) Å, b = 11.7305 (11) Å, c = 39.44121 (60) Å	a = 39.00313 (26) Å, b = 11.70259 (11) Å, c = 3.875918 (35) Å, β = 95.64781 (72) °
V (Å^3)	1798.07 (30) Å^3	1760.527 (46) Å^3
Z	2	2
D_x (g cm^{-3})	8.21	8.44
Radiation type	Cu *Kα*	
μ (mm^{-1})	88.421	91.297
Data collection		
Diffractometer	Rigaku Miniflex II	
θ–range	1.5–45, Step size (°) 0.02	1.5–35, Step size (°) 0.02
$(\sin \theta/\lambda)_{max}$ (Å^{-1})	0.459	0.372
Refinement		
R_{wp}	0.058	0.066
R_p	0.050	0.063
R_{Bragg}	0.067	0.089
S	1.73	4.06
No. of parameters	28	66

2.5. Band structure calculations

DFT calculations on the electronic structure of **2** ($Bi_{18}O_{22}Cl_8Se$) were performed using the projector augmented wave method (PAW) as implemented in the *Vienna Ab initio Simulation Package* (VASP) [42,43]. Ordered models with (i) alternating Se and Cl atoms in the Se1/Cl4 position, and (ii) pairwise –Cl–Cl–Se–Se– motif of the occupancy of that site were considered to describe mixed occupancy; the first model was found to be favorable by *ca*. 1.09 eV and therefore was used in the discussion. Experimental structure parameters were used for the calculations and transformed to the *P*1 group; in both cases, the relaxation of atomic coordinates was carried out to determine minimum structure and eliminate structural tension. The r^2SCAN exchange-correlation functional of the *meta*-GGA type was used for the calculations [44]. The number of *k*-points in the first Brillouin zone was chosen so as to provide a step between *k*-points of no more than 0.02 $Å^{-1}$. Energy cutoff was set to 500 eV, and the energy convergence criterion was at 10^{-5} eV. Charge density analysis was performed employing PAW augmentation using the Bader 1.04 package from Henkelman group [45–48]. DOS and band plots were produced using sumo 2.2.5 package [49].

2.6. Raman spectroscopy

The polarized Raman spectra of **1** were measured using a Bruker FT 100/S spectrometer with YAG:Nd laser excitation at 1064 nm. The spectral resolution was 2 cm^{-1}. The orientation of the crystallographic axes was done using the X–ray method; *x*–, *y*– and *z*–axes were taken as $x \parallel a$, $y \parallel b$ and $z \parallel c$.

3. Results

3.1. Crystal structures

The crystal structures of **1** and **2** can be regarded as comprised of relatively thick (~16 Å) layers comprised of double litharge–like sheets "reinforced" by ribbons cut out of the same litharge sheets, in the manner of steelwork; these layers are separated by anionic sheets of chloride and borate anions (Fig. 3). The metal–oxygen framework is formed by edge–sharing oxocentered OBi_4 (*d* (Bi–O) = 2.189–2.753 Å for **1** and 2.152–2.798 Å for **2**) tetrahedra; at the "junctions" of litharge layers and ribbons, OBi_5 are formed (*d* (Bi–O) = 2.21–2.78 Å for **1** and 2.25–2.81 Å for **2**). Some Bi–O distances are somewhat below average but observed, for instance, in the structure of $Bi_{24}O_{31}Cl_{10}$ [50]. Note that due to low symmetry of the structure and relatively weak scattering power, the positions of oxygen atoms are determined with lower precision. Within these "steelwork" junctions, seven oxocentered polyhedra (six OBi_4 and one OBi_5) form "clusters" (Fig. 3d). The bismuth–oxide framework features trigonal channels (Fig. 3e) filled by the Cl1 and Cl2 anions. The interlayer anionic sheets are filled by Cl3 and a mixed Cl4/B (1)O_3 site (75 % Cl^-, 25 % disordered BO_3^{3-} triangles (*d* (B–O) = 1.372–1.449 Å) (Fig. 3c) or mixed Cl4/Se1 site (50 % Cl^-, 50 % Se^{2-}). This low precision and scatter in the B–O distances is again due to the low occupancy and orientational disorder of the borate group so that the actual scattering from partly occupied oxygen sites is very low, particularly considering the high percentage of heavily scattering bismuth atoms and relatively low overall crystal symmetry.

The Cl1 and Cl2 atoms are coordinated by six bismuth atoms in a regular way (*d* (Bi–Cl) = 3.12–3.31 Å for **1** and 3.07–3.32 Å for **2**). The Cl3 and Cl4 center almost ideal Bi8 cubes (3.462 Å × 8, 3.380 Å × 4 + 3.396 Å × 4 for **1** and 3.365 Å × 8, 3.330 Å × 4 + 3.258 Å × 4 for **2**).

The calculated bond–valence sums [51] for Bi (2.57–3.31 v.u. for **1** and 2.92–3.38 v.u. for **2**), Cl (0.56–0.97 v.u. for **1** and 0.75–1.04 v.u. for **2**) and O (1.20–2.35 v.u.) are close to their formal valences. It is curious to note that in the OBi_5 species, the BVS of the oxygen atom is surprisingly low (1.20 v.u.), which may reflect certain strain at the junctions. We have also calculated the bond–valence energy landscape (BVEL) of **1** using the BondStr software [39] (Fig. 4); based on these results, it is possible to suggest that there is at least some free room to permit migration of the chloride anions along [100]. It should be noted note that the needle axis of the crystals corresponds to the [100] direction of their structure (Fig. 1b).

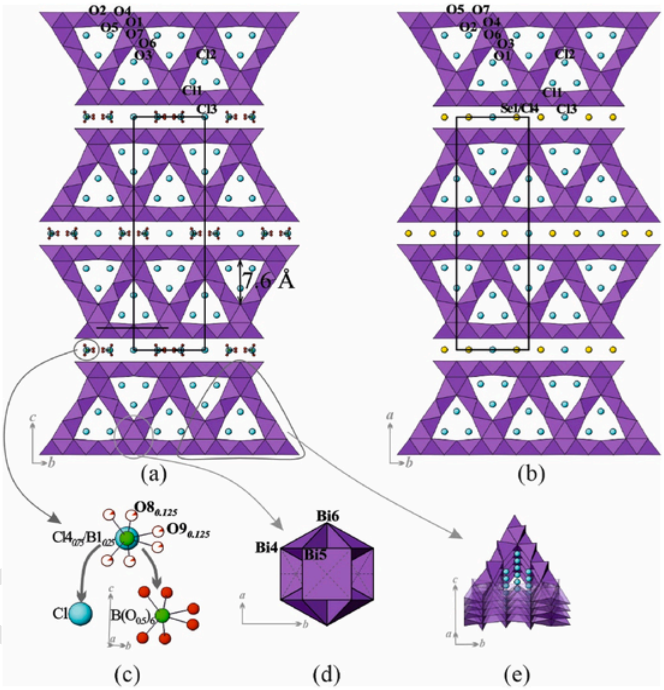

Fig. 3. Crystal structures of (a) **1** and (b) **2**. The mixed Se/Cl anionic site is highlighted in yellow; the "inviolable" Cl^- site is shown in green. (c) The joint–occupied position filled by disordered BO_3^{3-} and Cl^-, (d) association of the OBi_4 and OBi_5 oxocentered polyhedra in **1** and (e) Cl–bearing channels. The occupancies of the O8, O9, Cl4 and B1 sites are shown in italic subscripts.

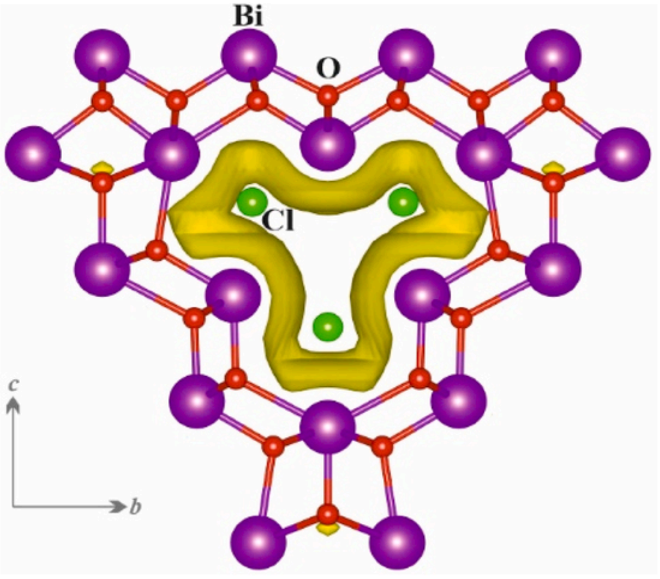

Fig. 4. Part of the structure of **1** with the suggested migration channels of the Cl^- anions. calculated in BondStr software [39].

CORRECTED P

The structure of **2** is very similar to the one described above but adopts monoclinic symmetry. The bond lengths in the OBi_4 units vary between 2.15 and 2.80 Å, while in the OBi_5 square pyramids, between 2.25 and 2.81 Å. Again, the BVS for the oxygen in OBi_5 is relatively low.

It is worth noting that the higher–charged Se^{2-} anion in **2** partially occupies the interlayer site equivalent to that occupied by the BO_3^{3-} species in the structure of **1** despite its size being much closer to that of Cl^-, and mixed Se^{2-}/Cl^- occupancy is observed over several anionic sites in the mixed–layer Sillén–type oxohaloselenides [17,18]. The other interlayer site as well as those inside the trigonal channels, remain occupied exclusively by Cl^-. This may be indicative of some structural restrictions not permitting incorporation of larger anionic species. This is in line with the negative results of attempting to substitute, even partially, Cl^- by slightly larger Br^- in these structures.

Following the rules developed for the description of ordered microporous and mesoporous materials with inorganic hosts approved by International Zeolite Association, the crystal chemical formulas of studied compounds should be written in the following order: |guest composition| [host composition] $_h${dimensionality of the host $\boldsymbol{D}^h$} $_p${dimensionality of the pore system $\boldsymbol{D}^p$ – shape of the pore $n_i^{m_i}$ – direction of the channel [*uvw*]} (symmetry) [52,53]. Consequently, the general crystal chemical formulas can be written as follows ($Z = 2$):

$$\left|\mathrm{Cl}_6\right|_{add}\left[(\mathrm{BO}_3)_{0.5}\mathrm{Cl}_{2.5}\right]\ \left[\mathrm{Bi}_{18}\mathrm{O}_{22}\right]\ _h\{2\}\ _p\left\{1\left[4^9 6^3 15^{2/2}\right][100](15-\mathrm{ring})\right\}$$

and

$$\left|\mathrm{Cl}_6\right|_{add}\left[\mathrm{SeCl}_2\right]\ \left[\mathrm{Bi}_{18}\mathrm{O}_{22}\right]\ _h\{2\}\ _p\left\{1\left[4^9 6^3 15^{2/2}\right][001](15-\mathrm{ring})\right\}\ (C2/m)$$

indicating that the 2**D** host structure consists of a system of parallel channels (filled by "guest" Cl^- anions) running either along [100] in (**1**) or [001] in (**2**) direction. Channels are characterized by the $[4^9 6^3 15^{2/2}]$ topology with the 15-membered ring (15R) pore opening. The additional layer of the compositions $[(BO_3)_{0.5}Cl_{2.5}]$in (**1**) or $[SeCl_2]$ in (**2**) in present between the adjacent 2**D** host structure.

3.2. Raman spectroscopy studies

The presence of tiny amounts of borate groups deduced from the structural was also conformed from Raman studies of single crystals of **1** (Fig. 5). Though the intensities of the corresponding bands are expectedly low, they are clearly seen in the inset. The peak at 701 cm^{-1} is attributed to the bending vibrations of BO_3 groups. The peak at 944 cm^{-1} is attributed to their symmetric stretching, while the asymmetric stretching mode of the BO_3 groups occurs at 1220 cm^{-1}. The peaks at 104–325 cm^{-1} are related to the Bi–O lattice vibrations and stretching frequencies of the BiO units with Bi–O bonds $<$2.4 Å. Peaks at 450, 495 cm^{-1} are related to the stretching frequencies of the BiO units with Bi–O bonds $>$2.4 Å. There is some distant correlation to the ~60, 150, and 200 cm^{-1} modes of BiOCl observed in Raman [54] and ~530 cm^{-1} in its IR spectrum [55].

3.3. On the presence of boron in the structure of 1

The localization of the weakly scattering and disordered BO_3 group in the structure of **1** in the presence of strong scatterers requires additional argumentation. We note that in the previous case of incommensurately modulated structure of Bi_4BO_7Cl we faced a similar pattern with the BO_3 groups and Cl atoms occupying the same position; yet, these were partially ordered which caused the structural modulation [29] In contrast, the structure of **1** exhibits full orientational and occupational BO_3/Cl disorder.

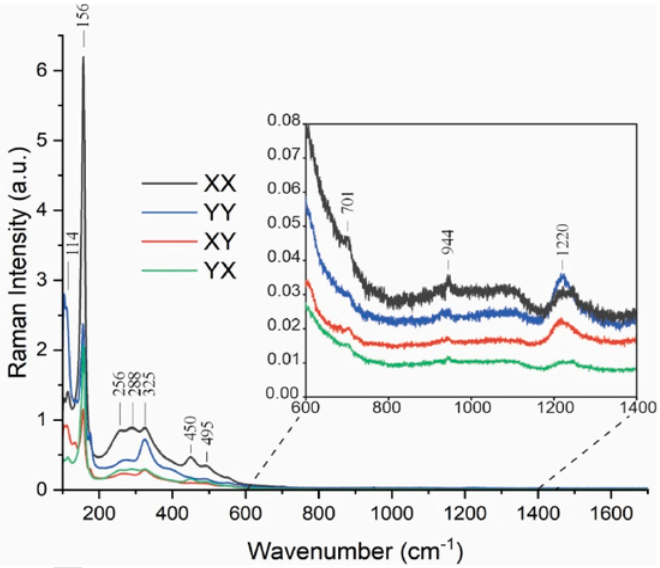

Fig. 5. Raman spectra of $Bi_{18}O_{22}Cl_{8.5}(BO_3)_{0.5}$.

The EDX spectroscopy data also do not provide convincing arguments, particularly in the case of suggested low boron content. The ratio of heavier elements, except boron, agrees well to the proposed composition. Yet, the Raman spectrum acquired from the crystals of **1** contain weak bands corresponding to the borate group. In addition, the compound **1** was not found on the phase diagram of Bi_2O_3 – $BiCl_3$ system [56]. Yet, addition of bismuth borate in the reaction mixture permits to prepare this compound with an essential yield.

3.4. Electronic structure of $Bi_{18}O_{22}Cl_8Se$

DFT calculations were performed on the compound **2**, as it is more ordered of the two and can be modeled more accurately. However, due to the similarities of the structures and the location of main structure-building blocks, we expect electronic structures of both compounds to be fairly similar.

The density of states (DOS) plot (Fig. 6) shows the compound to be a narrow-gap semiconductor. Atomic projection analysis indicates that the major contributions to the valence band near the Fermi level come from Cl *3p*, O *2p*, and Se *4p* states, with strong contribution from Bi *6p* states to the conduction band. The bottom of the conduction band is characterized by the region of very low, but non-zero DOS, implying that it is formed by very few bands as compared to the main contributions to both valence and conduction bands.

The DOS analysis is corroborated by the band plots (Figs. 7 and 8). As seen from the plots, the compound is an indirect-gap semiconductor with the band gap of *ca.* 0.18 eV. Valence band maximum (VBM) is at M point, and conduction band minimum (CBM) is at Γ point. The strongest contributions to VBM are provided by the Cl *3p* and O *2p* states, while Bi 6*p* states and Cl *2p* states feature most prominently in CBM. Fig. 8 shows only the contributions from Se1/Cl4 *p*-states and confirms that the atoms in the mixed position also contribute to CBM/VBM, although their contributions are minor. Generally, both CBM and VBM are formed by relatively few bands, which is consistent with the information provided by DOS analysis.

Bader charge density analysis indicates a significant degree of charge transfer from bismuth to the anionic part of the structure. Average calculated charges are: +2.75 (Bi), −0.90 (Cl), −1.13 (Se), −1.86 (O). Such high values indicate strongly ionic nature of the structure, with all the atoms except Se practically reaching their most stable positive (Bi) or negative (Cl, O) oxidation states. This charge distribution is

CORRECTED P

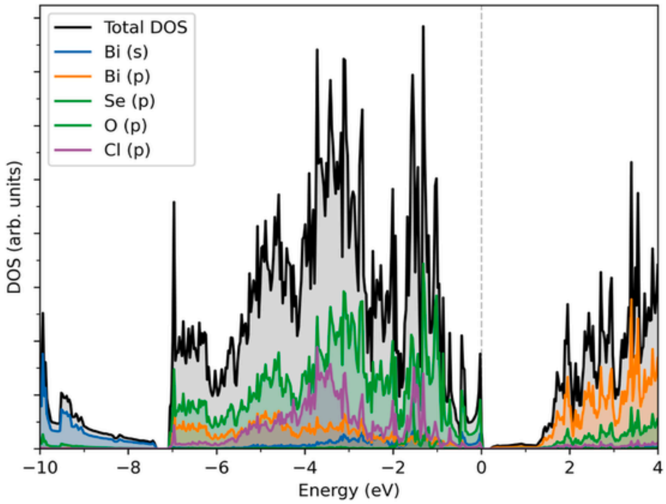

Fig. 6. Total and projected densities of states (DOS) near the Fermi level (marked by dotted line) for **2**.

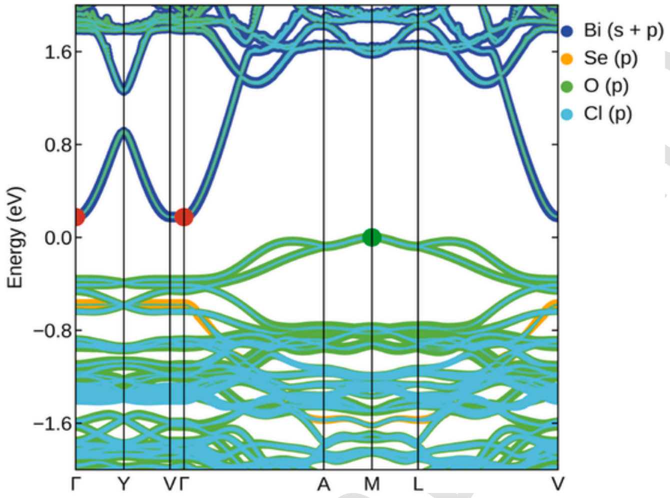

Fig. 7. Calculated band structure for **2**. The thickness of the lines is proportional to the size of the contribution. Fermi energy is at zero. Red dot marks conduction band minimum, green valence band maximum.

also consistent with DOS plots which show respective filled or vacant states for each element.

3.5. *Structural relationships between tunnel bismuth oxychlorides and lead fluorohalides*

The new compounds **1** and **2** are new members of a relatively large family of litharge–derived structures featuring trigonal or nearly trigonal channels filled by halide anions. Herein we present a brief review of its structural chemistry.

The nearest structural relative to **1** and **2** is the $PbBi_{17}O_{22}Cl_9$ oxychloride (Fig. 9e) [28] which contains the same "steelwork–reinforced" layers with a just slightly different composition. In this case, the positive charge of the layers is exactly compensated by the five fully occupied Cl sites. Though the difference in scattering by Bi^{3+} and Pb^{2+} is very small, the latter cations were assumed to occupy the cation sites at the junction points. In the structure of **1**, as well as of **2**, all cation sites are fully occupied by Bi^{3+} and their positive charge is compensated by

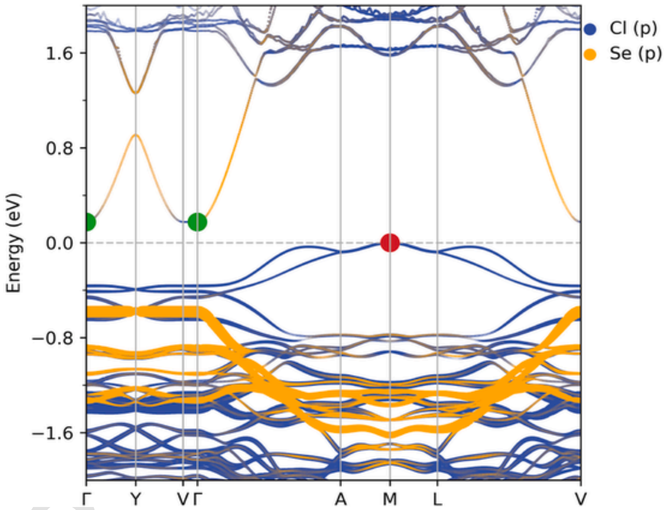

Fig. 8. Band projections for Se1 and Cl4 atoms in the structure of **2**. The thickness of the lines is proportional to the size of the contribution. Fermi energy is at zero. Red dot marks conduction band minimum, green valence band maximum.

partial substitution of Cl^- by a higher charged BO_3^{3-}. These anions are strictly localized in the interlayer space; this part of the structure is similar to that in $[Bi_4O_4](BO_3)Cl$ [29]. This substitution also leads to increase of symmetry from monoclinic ($PbBi_{17}O_{22}Cl_9$) to orthorhombic (**1**). In the meantime, **2** is a complete analog of $PbBi_{17}O_{22}Cl_9$ from which we conclude that the increase of symmetry in **1** is due to incorporation of a relatively large BO_3^{3-} anion which is able to form covalent bonds to the neighboring Bi atoms contrary to Se^{2-} and Cl^-. Further studies are evidently necessary to support this suggestion; yet, incorporating isoelectronic or isolobal analogs of BO_3^{3-} (CO_3^{2-} and NO_3^-) or Se^{2-} (S^{2-} and Te^{2-}) seems to be a synthetic challenge given the high synthesis temperature and overall thermal instability of carbonates and nitrates and high–temperature redox processes in the $Bi_2O_3 – Bi_2S_3$ and $Bi_2O_3 – Bi_2Te_3$ systems [55]. Note also that the corresponding bromides were not reported; our attempts to approach these were also not successful. As noted above, this indicates existence of some restrictions; even the structures of **1** and **2** may lie rather close to the crystal chemical "borderline" due to the presence of strained parts, most probably the $O(Bi,M)_5$ square pyramids.

In accordance with the IZA rules, the crystal chemical formula of $PbBi_{17}O_{22}Cl_9$ can be written as:

$$\left|\mathrm{Cl}_6\right|_{add}[\mathrm{Cl}_3]\ [\mathrm{PbBi}_{17}\mathrm{O}_{22}]\ _h\{2\}\ _p\left\{1\left[4^9 6^3 15^{2/2}\right][010](15-\mathrm{ring})\right\}(C2/m)$$

the topologies of the 2D host structure represented by the $\{|Cl_6|@[Bi_{18}O_{22}]\}$ in studied compounds (**1**) and (**2**) as well as $PbBi_{17}O_{22}Cl_9$ are the same and the main difference is the slight shift of the adjacent layers along the "additional" layer which is reflected in the symmetry of their structures. Thus, these compounds can be considered as polytypes and could described in the terms of OD ("order/disorder") approach [58,59]. Moreover, based on the TEM images [28] it is clear to see that the number of the "additional" {BiOCl} layers intercalating between $\{|Cl_6|@[Bi_{18}O_{22}]\}$ host layers could be different forming the modular series with the hypothetical simplified formula:

$$\left|X_6\right|_{add}\left[Y_3|(\mathrm{BiOCl})_n\right]\ [M_{18}\mathrm{O}_{22}]\ _h\{2\}\ _p\left\{1\left[4^9 6^3 15^{2/2}\right](15-\mathrm{ring})\right\}$$

where $X = Cl^-$; $Y \equiv Cl^-$, Se^{2-}, $(BO_3)^{3-}$; $M = Bi^{3+}$, Pb^{2+}; $n = 1, 2, 3$.

CORRECTED PROOF

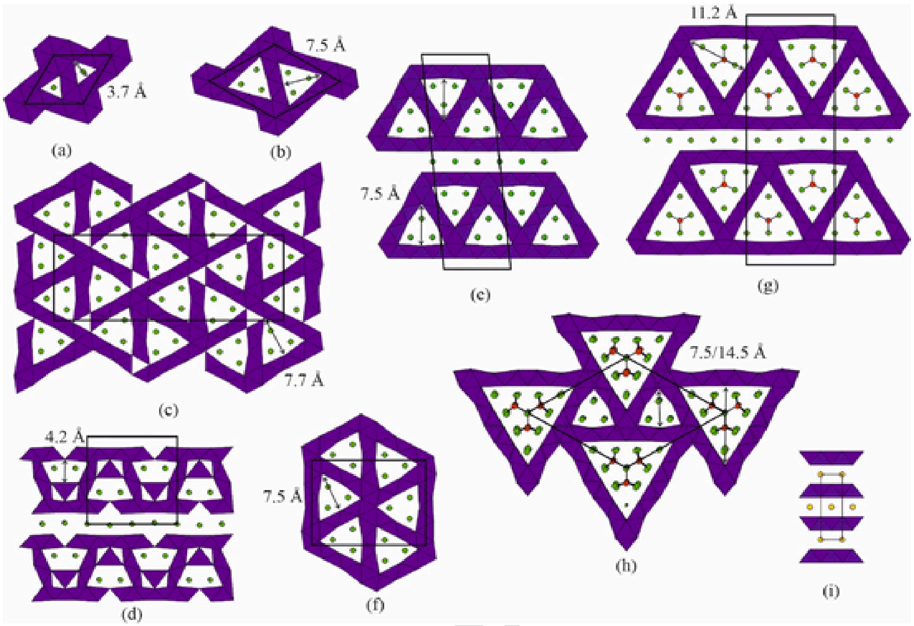

Fig. 9. The crystal structures of (a) $(PbF_2)_6PbCl_2$, (b) $Na_2Pb_{11}F_{18}Cl_6$ [57], (c) $Bi_{12}O_{15}Cl_6$, (d) $(Mn_{0.8},Pb_{0.2})Bi_9O_{12}Cl_5$ [28], (e) $PbBi_{17}O_{22}Cl_9$ [28], (f) $Bi_6O_7FCl_3$, (g) $NaBi_6O_{7.5}Cl_4$ [28], (h) $Ag_{4.78}Bi_{48}Cl_{31.5}O_{58.64}$ [26] and (i) Bi_2O_2Se [30]. The anion-centered polyhedra are shown in violet, the chloride anions at the interfaces, in green; the Na^+ and Ag^+ filling the interstices, in red. The arrows indicate the size of the channels which are shown nearby.

CORRECTED P

Significantly more complex is the structure of $NaBi_6O_{7.5}Cl_4$ (Fig. 9g) [28] which is also characterized by the **2D** host structure, with the trigonal cross-section, but with the notably wider with the effective channel width of 11.2 Å. The crystal chemical formula can be written as ($Z = 4$):

$$\left|(NaCl_3)\,Cl_3\right|_{add}[Cl_2]\ [NaBi_{12}O_{15}]\ {}_h\{2\}\ {}_p\{1\,[4^{15}6^{3}21^{2/2}]\,[100]\,(21-\mathrm{ring}$$

As the wide channels are filled by both Cl^- anions and ${}^{1}_{\infty}[NaCl_3]^{2-}$ anionic chains with the trigonal prismatic coordination of the central Na^+ cation, this structure can be considered as a “salt–inclusion”. The Na^+ cations also actively contribute to the formation of the “steelwork” layers and provide the overall charge balance; this is facilitated by the near equality of the ionic radii of Bi^{3+} (1.18 Å vs. 1.17 Å for the CN of 8 [60]) – most cationic sites are mixed–occupied. The sites at the junctions are partially disordered which again suggests an essential strain in this part of the structure.

The simplest representative of this kind of anion-centered layers is observed in the crystal structure of compound $(Mn_{0.8}Pb_{0.2})Bi_9O_{12}Cl_5$ [28] (Fig. 9d) which features essential distortions of the litharge motif at the junctions. This structure contains similar system of the parallel channels with the trigonal cross-section within the **2D** host structure filled only by Cl^- anions. The crystal chemical formula is ($Z = 4$):

$$\left|Cl_3\right|_{add}[Cl_2]\ [(Mn_{0.8}Pb_{0.2})\,Bi_9O_{12}]\ {}_h\{2\}\ {}_p\{1\,[4^{12}6^{2}16^{2/2}]\,[100]\,(16-\mathrm{rin}$$

The bismuth/lead oxides and oxohalcogenides also exhibit **3D** host structures represented by the “antizeolite” frameworks, formed by anion-centered polyhedra. Among them there is a group of compounds which structures adopt a hexagonal symmetry, so the “complete” litharge slabs are no longer present and, as the result, the **2D** layers transform to **3D** frameworks. The “antizeolite” crystal structures of $Bi_{12}O_{15}Cl_6$ (Fig. 9c) [24] and $Bi_6O_7FCl_3$ (Fig. 9f) [25] are characterized by the presence of system of parallel channels with the trigonal cross-section. However, their structures are formed by a slightly different way of “junctioning” the litharge ribbons of different width. Nevertheless, the topology of the channels in the crystal structure of $Bi_6O_7FCl_3$ (Fig. 9f) [25] is the same like in compound (**1**) ($Z = 2$):

$$\left|Cl_6\right|\ [Bi_{12}O_{14}F_2]\ {}_h\{3\}\ {}_p\{1\,[4^{9}6^{3}15^{2/2}]\,[010]\,(15-\mathrm{ring})\}\ (Pnma)$$

Despite the same amount of bismuth cations and rather similar stoichiometry between $Bi_{12}O_{14}F_2Cl_6$ ($=Bi_6O_7FCl_3$ [25]) and $Bi_{12}O_{15}Cl_6$ [24], the decreasing number of anions forming the “antizeolite” framework by the $2F^- \rightarrow O^{2-}$ substitution significantly changes the topology of the channels. Later, Hopfgarten [61] suggested the existence of a third member of this family containing both “intact” litharge slabs and ribbons, however, no experimental evidence exists for this structure.

Essentially more complex “antizeolite” frameworks with two systems of parallel channels are present in the structures of $Bi_{48}O_{59}Cl_{30}$ (M_5Cl) (M = Cu, Ag) (Fig. 9h) [26]. Both channels are characterized by trigonal cross-sections wherein the first one (topologically equal to that in (**1**) and related compounds) is filled only by Cl^-, while the second one is filled non-stoichiometric copper-chlorine salt inclusion. The non-stoichiometry of the salt–inclusion parts suggests a possible cation migration along the wide channels of the second type. Taking into account the presence of two types of the channels as well as the non-stoichiometry of the oxygens the corresponding idealized crystal chemical formula can be written as:

$$\left|Cu_5Cl_{30}\right|\ [Bi_{48}O_{60-x}]\ {}_h\{3\}\ {}_p\left\{\begin{array}{l}1\,[4^{9}6^{3}15^{2/2}]\,[001]\,(15-\mathrm{ring})\\ 1\,[4^{21}6^{3}27^{2/2}]\,[001]\,(27-\mathrm{ring})\end{array}\right\}\ (P\bar{6}2m$$

where $x = 1$. Note that bromide analogs for these oxychlorides featuring small trigonal channels have not been reported as well.

Isoelectronic to the Bi^{3+}/O^{2-} is the Pb^{2+}/F^- couple which also very commonly contributes to the litharge slabs. The crystal structures of compounds with the general formula $M_2Pb_{11}F_{18}X_6$, where M = Na, K and X = Cl, Br [57] also contain two system of parallel channels with

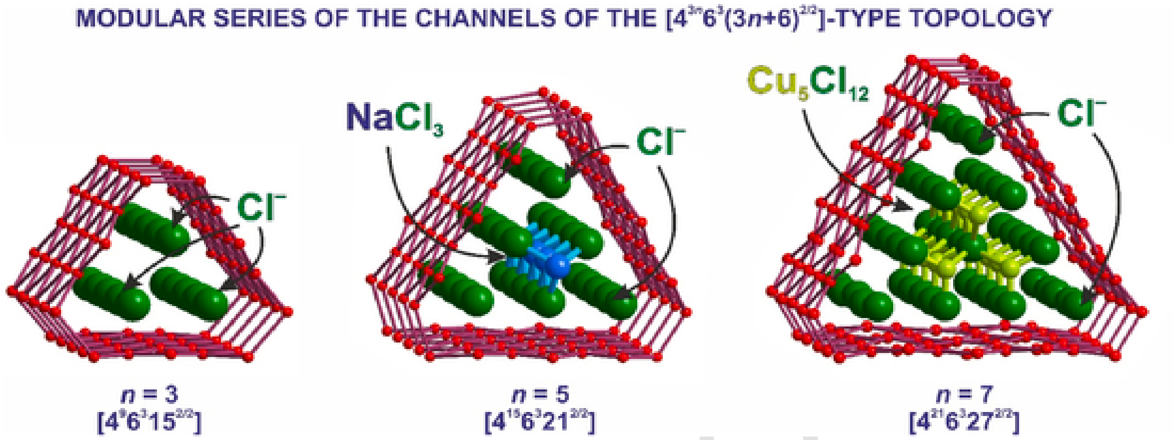

Fig. 10. Different types of the channel topologies of anion-centered tetrahedra.

the trigonal and hexagonal (topologically equal to those in the crystal structures of **1** and **2**) cross-sections, filled by X^{-}_{6} and M^{+} guests (Fig. 9b). All the framework sites are jointly occupied by M^{+} and Pb^{2+} cations. Thus, the crystal chemical formula can be written as:

$$\left|MX_6\right| \; [M\mathrm{Pb}_{11}\mathrm{F}_{18}]\ {}_{h}\{3\}\ {}_{p}\left\{\begin{array}{c} 1\left[4^9 6^3 15^{2/2}\right][001]\,(15-\mathrm{ring}) \\ 1\left[4^2 6^{2/2}\right][001]\,(6-\mathrm{ring}) \end{array}\right\}(P6_3/m)$$

In this cases, formation of bromides (but not iodides) is possible due to the larger size of Pb^{2+} compared to Bi^{3+} (the radii of O^{2-} and F^{-} are nearly the same).

Most of the tunnel bismuth/lead oxychlorides are characterized by the presence of the rather similar channels with the trigonal cross-section which topologies can be described by the general formula $[4^{3n}6^3\ (3n+6)^{2/2}]$ (Fig. 10) where $n = 3$ (**2D**-zeolite-related compounds (**1**), (**2**), and $PbBi_{17}O_{22}Cl_9$ [28]; “anti-zeolites” $Bi_6O_7FCl_3$ [25], $Bi_{48}O_{59}Cl_{30}(M_5Cl)$ (M = Cu, Ag) [26] and $M_2Pb_{11}F_{18}X_6$, (M = Na, K; X = Cl, Br) [57]), $n = 5$ ($NaBi_6O_{7.5}Cl_4$ [28]), and $n = 7$ ($Bi_{48}O_{59}Cl_{30}(M_5Cl)$ (M = Cu, Ag) [26]). Such relation indicates a polysomatic and modular aspect [58,59] of the crystal structures of bismuth/lead oxychlorides similar to that in the crystal structures of tunnel manganese oxides [53]. Depending on the effective channel width they could be filled either by Cl^{-} anions or more complex anions with “salt-inclusion” structure.

4. Discussion

There are several points about the crystal chemistry of this unusual family which are worth noting. First, the environment of the majority of the cationic sites corresponds to the Archimedean $(Bi,M)O_4Cl_4$ or $(Pb,M)F_4X_4$ (X = Cl, or Br) as in the “archetypic” X_1–type Sillén structure, $[M_2(O,F)_2]X$ (Fig. 9i) [62,63]. Hence, these structures can be regarded also as its complex derivatives. Second, there is a likely size match between the size of the cannels and the radius of the corresponding halide anion. With the smaller Bi^{3+}–O^{2-} pair, the channels can be filled by only Cl^{-}; no bromide analog of any structure reported above is known (note that most Cl positions in the structures of **1** and **2** are “closed” to substitution by larger species). While crystals of **1** were obtained as a minute admixture to Bi_4BO_7Cl, the corresponding Bi_4BO_7Br and Bi_4BO_7I compounds were produced phase–pure under the same synthesis conditions. With the larger Pb^{2+}–F^{-} pair, the size of the trigonal channels is large enough to home Br^{-}, but yet not by I^{-}; this is in vivid contrast to the corresponding layered archetypes wherein the interlayer space readily hosts Cl^{-}, Br^{-}, and I^{-} with minimal, if any, variation of the structure [12,14].

It should be noted however, as we briefly mentioned above, that the chemistry of the multi–anion bismuth oxyhalides is yet at the early stages of its development and many new compounds which now seem unusual are expected to be discovered and explained. The seemingly relatively simple Bi_2O_3 – $BiCl_3$ – Bi_2Se_3 system, initially explored by Schmidt et al., was shown to contain three pseudo–ternary compounds, $Bi_4O_4SeCl_2$, $Bi_{10}O_{12}SeCl_4$, and $Bi_{22}O_{28}SeCl_8$ [64]; for the latter compounds, Arppé-like structures were suggested. Later studies, dedicated mostly to Sillén–like layered structures, confirmed existence of the former compound and revealed two new representatives, $Bi_6O_6Se_2Cl_2$ and a disordered mixed–layer compound $Bi_8O_8Se_3Cl_2$ [18]; our studies in the same system produced the new compound **2**. This suggests that either some compositions were initially misidentified or, hopefully, there are some more pseudo–ternaries within the system which were not discovered at the earlier studies due to some kinetic hindrances. Note that the multi–anionic $Bi_4O_4SeCl_2$ and $Bi_6O_6Se_2Cl_2$ are full structural analogs of multi–cationic $MBi_3O_4X_3$ (M = Pb, Sr) and $M_2Bi_4O_4Br_6$ (M = Ca, Sr, Cd) [5,6,65,66]. Very close structural relationships between $PbBi_{17}O_{22}Cl_9$, **1**, and **2** testify that these structural analogies are indeed not unique for the Sillén–type structures but stretch much further into the realm of much more complex architectures. The suggested structural relationships of the yet not characterized $Bi_{10}O_{12}SeCl_4$, and $Bi_{22}O_{28}SeCl_8$ compounds to the “Arppé phases” $Bi_{24}O_{31}X_{10}$ are in line with this suggestion.

The tunnel oxides are characterized by the wide structural diversities and the effective size of the channels [67]. Most of them belong to a large family of manganese oxides with modular structures and different types of the porosity [68–70] and attract interests as charge storage materials for rechargeable batteries and supercapacitors, since the tunnels enable fast reversible insertion/extraction of charge carriers [71–73]. The considered families of microporous bismuth oxide can be analogs of the octahedral molecular sieves with the host structures formed by the anion-centered polyhedra. As the frameworks are positively-charged these compounds can be considered as the possible matrix for the storage of large anions, such as radioactive ^{36}Cl.

Funding sources

Synthesis, EDX analysis, crystal structure determination, Raman measurements, powder X-ray diffraction were financially supported by the Russian Science Foundation through Grant 22–13–00317.

CORRECTED PRO

Accession codes

CCDC 2331636 and 2331637 contain the supplementary crystallographic data for this paper. These data can be obtained free of charge via www.ccdc.cam.ac.uk/data_request/cif, or by emailing data_request@ccdc.cam.ac.uk, or by contacting The Cambridge Crystallographic Data Centre, 12 Union Road, Cambridge CB2 1EZ, UK; fax: +44 1223 336033.

CRediT authorship contribution statement

Dmitri O. Charkin: Writing – original draft, Formal analysis, Conceptualization. **Sergey N. Volkov:** Writing – original draft, Investigation, Formal analysis, Conceptualization. **Alexey N. Kuznetsov:** Writing – original draft, Investigation, Formal analysis. **Alexey Povolotskiy:** Investigation, Formal analysis. **Anastasia P. Chernyatieva:** Formal analysis. **Julia S. Mironova:** Formal analysis. **Sergey M. Aksenov:** Writing – original draft, Supervision, Formal analysis, Conceptualization.

Declaration of competing interest

The authors declare that they have no known competing financial interests or personal relationships that could have appeared to influence the work reported in this paper.

Data availability

No data was used for the research described in the article.

Appendix A. Supplementary data

Supplementary data to this article can be found online at https://doi.org/10.1016/j.jssc.2024.124889.

References

[1] C.A.-P. de Araujo, J.D. Cuchiaro, L.D. McMillan, M.C. Scott, J.F. Scott, Fatigue-free ferroelectric capacitors with platinum electrodes, Nature 374 (1995) 627–629, https://doi.org/10.1038/374627a0.

[2] X. Liu, P. Long, Z. Sun, Z. Yi, Optical, electrical and photoelectric properties of layered-perovskite ferroelectric Bi_2WO_6 crystals, J Mater Chem C Mater 4 (2016) 7563–7570, https://doi.org/10.1039/C6TC02069K.

[3] W. Ueda, J.M. Thomas, Bismuth-rich layered solids as catalysts for the oxidation of methane to higher hydrocarbons, J. Chem. Soc. Chem. Commun. (1988) 1148, https://doi.org/10.1039/c39880001148.

[4] S.W. Lin, Y.C. Kim, W. Ueda, Complex metal halide oxides (2). Layered complex metal chloride oxides having the X1X2 structure as catalysts for the oxidative dehydrogenation of ethane, Bull. Chem. Soc. Jpn. 71 (1998) 1089–1094, https://doi.org/10.1246/bcsj.71.1089.

[5] H. Suzuki, M. Higashi, O. Tomita, Y. Ishii, T. Yamamoto, D. Kato, T. Kotani, D. Ozaki, S. Nozawa, K. Nakashima, K. Fujita, A. Saeki, H. Kageyama, R. Abe, $PbBi_3O_4X_3$ (X = Cl, Br) with single/double halogen layers as a photocatalyst for visible-light-driven water splitting: impact of a halogen layer on the band structure and stability, Chem. Mater. 33 (2021) 9580–9587, https://doi.org/10.1021/acs.chemmater.1c02876.

[6] Y. Ishii, H. Suzuki, K. Ogawa, O. Tomita, A. Saeki, R. Abe, Improved water oxidation activity of a Sillén $SrBi_3O_4Cl_3$ photocatalyst by flux method with an appropriate binary-component molten salt, Sustain. Energy Fuels 6 (2022) 3263–3270, https://doi.org/10.1039/D2SE00635A.

[7] X. Wei, M.U. Akbar, A. Raza, G. Li, A review on bismuth oxyhalide based materials for photocatalysis, Nanoscale Adv. 3 (2021) 3353–3372, https://doi.org/10.1039/D1NA00223F.

[8] Y. Peng, L. Xu, J. Peng, T. Wang, Q. Wang, Y. Li, Z. Yin, J. Han, J. Qiu, Z. Yang, Z. Song, Enhanced upconversion luminescence in layered $Bi_2GdO_4Cl{:}Yb^{3+}/Er^{3+}$ by reducing OVs and its application in photocatalysis, J. Lumin. 252 (2022) 119269, https://doi.org/10.1016/j.jlumin.2022.119269.

[9] J.A. Newnham, T. Zhao, Q.D. Gibson, T.D. Manning, M. Zanella, E. Mariani, L.M. Daniels, J. Alaria, J.B. Claridge, F. Corà, M.J. Rosseinsky, Band structure engineering of $Bi_4O_4SeCl_2$ for thermoelectric applications, ACS Organic & Inorganic Au 2 (2022) 405–414, https://doi.org/10.1021/acsorginorgau.2c00018.

[10] S.M. Aksenov, N.A. Yamnova, E.Yu Borovikova, A.S. Volkov, D.A. Ksenofontov, O.V. Dimitrova, O.A. Gurbanova, D.V. Deyneko, F. Dal Bo, P.C. Burns, $Bi_3(PO_4)O_3$, the simplest bismuth(III) oxophosphate: synthesis, IR spectroscopy, crystal structure, and structural complexity, Inorg. Chem. 57 (2018) 6799–6802, https://doi.org/10.1021/acs.inorgchem.8b01195.

[11] S.V. Krivovichev, O. Mentré, O.I. Siidra, M. Colmont, S.K. Filatov, Anion-centered tetrahedra in inorganic compounds, Chem. Rev. 113 (2013) 6459–6535, https://doi.org/10.1021/cr3004696.

[12] J. Olchowka, H. Kabbour, M. Colmont, M. Adlung, C. Wickleder, O. Mentré, $ABiO_2X$ (A = Cd, Ca, Sr, Ba, Pb; X = halogen) *sillen* X1 series: polymorphism versus optical properties, Inorg. Chem. 55 (2016) 7582–7592, https://doi.org/10.1021/acs.inorgchem.6b01024.

[13] J. Di, J. Xia, H. Li, S. Guo, S. Dai, Bismuth oxyhalide layered materials for energy and environmental applications, Nano Energy 41 (2017) 172–192, https://doi.org/10.1016/j.nanoen.2017.09.008.

[14] D.O. Charkin, Modular approach as applied to the description, prediction, and targeted synthesis of bismuth oxohalides with layered structures, Russ. J. Inorg. Chem. 53 (2008) 1977–1996, https://doi.org/10.1134/S0036023608130019.

[15] Z. Zhu, F. Chen, N. Tian, Y. Zhang, H. Huang, Bi-based layered perovskite oxyhalides: up-and-coming catalysts for efficient energy harvesting and conversion, Curr. Opin. Green Sustainable Chem. 37 (2022) 100669, https://doi.org/10.1016/j.cogsc.2022.100669.

[16] Q.D. Gibson, M.S. Dyer, G.F.S. Whitehead, J. Alaria, M.J. Pitcher, H.J. Edwards, J.B. Claridge, M. Zanella, K. Dawson, T.D. Manning, V.R. Dhanak, M.J. Rosseinsky, $Bi_4O_4Cu_{1.7}Se_{2.7}Cl_{0.3}$: intergrowth of BiOCuSe and Bi_2O_2Se stabilized by the addition of a third anion, J. Am. Chem. Soc. 139 (2017) 15568–15571, https://doi.org/10.1021/jacs.7b06168.

[17] Q.D. Gibson, T.D. Manning, M. Zanella, T. Zhao, P.A.E. Murgatroyd, C.M. Robertson, L.A.H. Jones, F. McBride, R. Raval, F. Cora, B. Slater, J.B. Claridge, V.R. Dhanak, M.S. Dyer, J. Alaria, M.J. Rosseinsky, Modular Design via Multiple Anion Chemistry of the High Mobility van der Waals Semiconductor $Bi_4O_4SeCl_2$, J. Am. Chem. Soc. 142 (2020) 847–856, https://doi.org/10.1021/jacs.9b09411.

[18] R. Ji, M. Lei, C. Genevois, W. Zhang, X. Ming, L. He, M. Allix, C. Yin, X. Kuang, X. Xing, Multiple Anion Chemistry for Ionic Layer Thickness Tailoring in $Bi_{2+2n}O_{2+2n}Se_nX_2$ (X = Cl, Br) van der Waals Semiconductors with Low Thermal Conductivities, Chem. Mater. 34 (2022) 4751–4764, https://doi.org/10.1021/acs.chemmater.2c00786.

[19] S.V. Rashchenko, T.B. Bekker, Crystal chemistry of novel "antizeolite" structures, J. Struct. Chem. 62 (2021) 1935–1945, https://doi.org/10.1134/S002247662112012X.

[20] A.P. Topnikova, T.A. Eremina, E.L. Belokoneva, O.V. Dimitrova, A.S. Volkov, S.M. Aksenov, Synthesis, crystal structure and topological features of microporous "anti-zeolite" $Yb_3(BO_3)(OH)_6{\bullet}2.1H_2O$, A new cubic borate with isolated BO_3 groups, Microporous Mesoporous Mater. 300 (2020) 110147, https://doi.org/10.1016/j.micromeso.2020.110147.

[21] A. Hyman, A. Perloff, The crystal structure of bismuth (2:1) borate, $2Bi_2O_3{\bullet}B_2O_3$, Acta Crystallogr. B 28 (1972) 2007–2011, https://doi.org/10.1107/S0567740872005436.

[22] U. Eggenweiler, J. Ketterer, E. Keller, V. Krämer, The crystal structure of α-Bi5O7I, Z. für Kristallogr. - Cryst. Mater. 216 (2001) 230–233, https://doi.org/10.1524/zkri.216.4.230.23259.

[23] M.G. Francesconi, A.L. Kirbyshire, C. Greaves, O. Richard, G. Van Tendeloo, Synthesis and structure of $Bi_{14}O_{20}(SO_4)$, A new bismuth oxide sulfate, Chem. Mater. 10 (1998) 626–632, https://doi.org/10.1021/cm9706255.

[24] F. Hopfgarten, The crystal structure of $Bi_{12}O_{15}Cl_6$, Acta Crystallogr. B 32 (1976) 2570–2573, https://doi.org/10.1107/S0567740876008285.

[25] F. Hopfgarten, The crystal structure of $Bi_6O_7FCl_3$, Acta Crystallogr. B 31 (1975) 1087–1092, https://doi.org/10.1107/S0567740875004554.

[26] B. Aurivillius, J. Albertsson, G. Svensson, L. Eberson, P. Krogsgaard-Larsen, K. Maartmann-Moe, S. Wold, Crystal structures of $\sim[M_5^ICl][Bi_{48}O_{59}Cl_{30}]$, M^I = Cu, Ag, Acta Chem. Scand. 44 (1990) 111–122, https://doi.org/10.3891/acta.chem.scand.44-0111.

[27] Ö. Sävborg, Structures of niobium and tantalum oxide fluorides containing lone-pair ions, J. Solid State Chem. 57 (1985) 154–159, https://doi.org/10.1016/S0022-4596(85)80004-9.

[28] M. Lü, A. Aliev, J. Olchowka, M. Colmont, M. Huvé, C. Wickleder, O. Mentré, Multidimensional open-frameworks: combinations of one-dimensional channels and two-dimensional layers in novel Bi/M oxo-chlorides, Inorg. Chem. 53 (2014) 528–536, https://doi.org/10.1021/ic402578m.

[29] S. Volkov, M. Arsent'ev, V. Ugolkov, A. Povolotskiy, Y. Savchenko, M. Krzhizhanovskaya, R. Bubnova, S. Aksenov, When the difference between incommensurate and commensurate structures becomes elusive: the case of Bi_4BO_7X (X = Cl, Br) oxyhalides, J. Appl. Crystallogr. 56 (2023) 589–596, https://doi.org/10.1107/S1600576723002261.

[30] H. Boller, Die Kristallstruktur von Bi_2O_2Se, Monatsh. Chem. 104 (1973) 916–919, https://doi.org/10.1007/BF00903904.

[31] D.J. Segal, B.P. Santoro, R.E. Newnham, Neutron-diffraction study of $Bi_4Si_3O_{12}$, Z. für Kristallogr. - Cryst. Mater. 123 (1966), https://doi.org/10.1524/zkri.1966.123.16.73.

[32] T.G.G. Battye, L. Kontogiannis, O. Johnson, H.R. Powell, A.G.W. Leslie, *iMOSFLM* : a new graphical interface for diffraction-image processing with *MOSFLM*, Acta Crystallogr D Biol Crystallogr 67 (2011) 271–281, https://doi.org/10.1107/S0907444910048675.

[33] P. Evans, Scaling and assessment of data quality, Acta Crystallogr D Biol Crystallogr 62 (2006) 72–82, https://doi.org/10.1107/S0907444905036693.

[34] L. Palatinus, G. Chapuis, *Superflip* – a computer program for the solution of crystal structures by charge flipping in arbitrary dimensions, J. Appl. Crystallogr. 40 (2007) 786–790, https://doi.org/10.1107/S0021889807029238.

[35] V. Petříček, L. Palatinus, J. Plášil, M. Dušek, Jana2020 – a new version of the crystallographic computing system Jana, Z. für Kristallogr. - Cryst. Mater. 0 (2023),

UNCORRECTED PROOF

https://doi.org/10.1515/zkri-2023-0005.

[36] K. Momma, F. Izumi, *Vesta* : a three-dimensional visualization system for electronic and structural analysis, J. Appl. Crystallogr. 41 (2008) 653–658, https://doi.org/10.1107/S0021889808012016.

[37] E. Dowty, ATOMS for Windows; Version 6.1; Shape Software: Kingsport, TN, USA, 2000.

[38] I.D. Brown, D. Altermatt, Bond-valence parameters obtained from a systematic analysis of the inorganic crystal structure database, Acta Crystallogr. B 41 (1985) 244–247, https://doi.org/10.1107/S0108768185002063.

[39] J. Rodriguez-Carvajal, BONDSTR-program for Distance, Angle and Bond Strength Calculations, 1995.

[40] J. Rodríguez-Carvajal, Recent advances in magnetic structure determination by neutron powder diffraction, Phys. B Condens. Matter 192 (1993) 55–69, https://doi.org/10.1016/0921-4526(93)90108-I.

[41] R.S. Bubnova, V.A. Firsova, S.N. Volkov, S.K. Filatov, RietveldToTensor: program for processing powder X-ray diffraction data under variable conditions, Glass Phys. Chem. 44 (2018) 33–40, https://doi.org/10.1134/S1087659618010054.

[42] G. Kresse, D. Joubert, From ultrasoft pseudopotentials to the projector augmented-wave method, Phys. Rev. B 59 (1999) 1758–1775, https://doi.org/10.1103/PhysRevB.59.1758.

[43] G. Kresse, J. Furthmüller, Vienna Ab Initio Simulation Package (VASP), v.5.4.4, (n.d.)..

[44] J.W. Furness, A.D. Kaplan, J. Ning, J.P. Perdew, J. Sun, Accurate and numerically efficient r ^{2} SCAN meta-generalized gradient approximation, J. Phys. Chem. Lett. 11 (2020) 8208–8215, https://doi.org/10.1021/acs.jpclett.0c02405.

[45] W. Tang, E. Sanville, G. Henkelman, A grid-based Bader analysis algorithm without lattice bias, J. Phys. Condens. Matter 21 (2009) 084204, https://doi.org/10.1088/0953-8984/21/8/084204.

[46] E. Sanville, S.D. Kenny, R. Smith, G. Henkelman, Improved grid-based algorithm for Bader charge allocation, J. Comput. Chem. 28 (2007) 899–908, https://doi.org/10.1002/jcc.20575.

[47] G. Henkelman, A. Arnaldsson, H. Jónsson, A fast and robust algorithm for Bader decomposition of charge density, Comput. Mater. Sci. 36 (2006) 354–360, https://doi.org/10.1016/j.commatsci.2005.04.010.

[48] M. Yu, D.R. Trinkle, Accurate and efficient algorithm for Bader charge integration, J. Chem. Phys. 134 (2011), https://doi.org/10.1063/1.3553716.

[49] A. M Ganose, A.J. Jackson, D. O Scanlon, sumo: command-line tools for plotting and analysis of periodic ab initio calculations, J. Open Source Softw. 3 (2018) 717, https://doi.org/10.21105/joss.00717.

[50] A. Aliev, J. Olchowka, M. Colmont, E. Capoen, C. Wickleder, O. Mentré, New $[PbBi_2O_4][Bi_2O_2]Cl_2$ and $[Pb_nBi_{10\text{-}n}O_{13}][Bi_2O_2]_nCl_{4+n}$ series by association of sizable subunits: relationship with arppe's compound $Bi_{24}O_{31}Cl_{10}$ and luminescence properties, Inorg. Chem. 52 (2013) 8427–8435, https://doi.org/10.1021/ic4002708.

[51] N.E. Brese, M. O'Keeffe, Bond-valence parameters for solids, Acta Crystallogr. B 47 (1991) 192–197, https://doi.org/10.1107/S0108768190011041.

[52] L.B. McCusker, F. Liebau, G. Engelhardt, Nomenclature of structural and compositional characteristics of ordered microporous and mesoporous materials with inorganic hosts, Microporous Mesoporous Mater. 58 (2003) 3–13, https://doi.org/10.1016/S1387-1811(02)00545-0.

[53] F. Liebau, Ordered microporous and mesoporous materials with inorganic hosts: definitions of terms, formula notation, and systematic classification, Microporous Mesoporous Mater. 58 (2003) 15–72, https://doi.org/10.1016/S1387-1811(02)00546-2.

[54] A. Rulmont, Raman spectra of a single crystal of BiOCl, Spectrochim. Acta A30 (1974) 311–313, https://doi.org/10.1016/0584-8539(74)80235-7.

[55] L. Ye, C. Gong, J. Liu, L. Tian, T. Peng, K. Deng, L. Zan, $Bin(Tu)_xCl_{3n}$: a novel sensitizer and its enhancement of BiOCl nanosheets' photocatalytic activity, J. Mater. Chem. 22 (2012) 8354, https://doi.org/10.1039/c2jm16829d.

[56] P. Schmidt, O. Rademacher, H. Oppermann, Untersuchung der Phasenbeziehungen in quaternären Systemen $Bi_2O_3/Bi_2Ch'_3/Bi2Ch\{''\}_3$ (Ch = S, Se, Te), Z. Anorg. Allg. Chem. 625 (1999) 255–261, https://doi.org/10.1002/(SICI)1521-3749(199902)625:2<255::AID-ZAAC255>3.0.CO;2-6.

[57] F. Kubel, A. Rief, Disorder in alkali lead fluorides $Na_{2-x}K_xPb_{11}F_{18}X_6$ with X = Cl, Br, Z. für Kristallogr. - Cryst. Mater. 221 (2006) 600–605, https://doi.org/10.1524/zkri.2006.221.8.600.

[58] G. Ferraris, E. Makovicky, S. Merlino, Crystallography of Modular Materials, Oxford University Press, 2008, https://doi.org/10.1093/acprof:oso/9780199545698.001.0001.

[59] S.M. Aksenov, D.O. Charkin, A.M. Banaru, D.A. Banaru, S.N. Volkov, D.V. Deineko, A.N. Kuznetsov, R.K. Rastsvetaeva, N.V. Chukanov, B.B. Shkurskii, N.A. Yamnova, Modularity, polytypism, topology, and complexity of crystal structures of inorganic compounds, J. Struct. Chem. 64 (2023) 1797–2028, https://doi.org/10.1134/S0022476623100013.

[60] R.D. Shannon, Revised effective ionic radii and systematic studies of interatomic distances in halides and chalcogenides, Acta Crystallogr., Sect. A A32 (1976) 751–767, https://doi.org/10.1107/S0567739476001551.

[61] F. Hopfgarten, The structures of $Bi_6O_7FCl_3$ and $Bi_{12}O_{15}C_{16}$ in relation to the hypothetical non-stoichiometric parent structure $Bi_6X_{7+n}Cl_3$, Acta Crystallogr. B 33 (1977) 952–953, https://doi.org/10.1107/S0567740877005147.

[62] J. Ketterer, V. Krämer, Structural characterization of the synthetic perites $PbBiO_2X$, X = I, Br, Cl, Mater. Res. Bull. 20 (1985) 1031–1036, https://doi.org/10.1016/0025-5408(85)90201-6.

[63] J.F. Ackerman, Preparation and luminescence of Pb_2OFX; X = Cl, Br, I, Mater. Res. Bull. 18 (1983) 1129–1132, https://doi.org/10.1016/0025-5408(83)90156-3.

[64] P. Schmidt, H. Oppermann, N. Söger, M. Binnewies, A.N. Rykov, K.O. Znamenkov, A.N. Kuznetzov, B.A. Popovkin, Gasphasengleichgewichte quaternärer bismut-selen-oxidchloride, Z. Anorg. Allg. Chem. 626 (2000) 2515–2524, https://doi.org/10.1002/1521-3749(200012)626:12<2515::AID-ZAAC2515>3.0.CO;2-Y.

[65] L.G. Sillén, A.S. Gjörling-Husberg, Röntgenuntersuchung von Calcium/Wismutoxychloriden und -oxybromiden, Z. Anorg. Allg. Chem. 248 (1941) 121–134, https://doi.org/10.1002/zaac.19412480203.

[66] L.G. Sillén, Die Kristallstruktur einiger Strontium- Wismutoxyhalogenide $[SrBi_3O_4Cl_3$, $SrBiO_2Br$, $SrBi_2O_3Br_2$ und $SrBi_3O_4Br_3]$, Z. Anorg. Allg. Chem. 246 (1941) 115–130, https://doi.org/10.1002/zaac.19412460201.

[67] M. Pasero, A short outline of the tunnel oxides, Rev. Mineral. Geochem. 57 (2005) 291–305.

[68] Y. Yuan, C. Liu, B.W. Byles, W. Yao, B. Song, M. Cheng, Z. Huang, K. Amine, E. Pomerantseva, R. Shahbazian-Yassar, J. Lu, Ordering heterogeneity of $[MnO_6]$ octahedra in tunnel-structured MnO2 and its influence on ion storage, Joule 3 (2) (2019) 471–484.

[69] Y. Yuan, K. He, B.W. Byles, C. Liu, K. Amine, J. Lu, E. Pomerantseva, R. Shahbazian-Yassar, Deciphering the atomic patterns leading to MnO_2 polymorphism, Chem 5 (7) (2019) 1793–1805.

[70] X. Hu, D.A. Kitchaev, L. Wu, B. Zhang, Q. Meng, A.S. Poyraz, A.C. Marschilok, E.S. Takeuchi, K.J. Takeuchi, G. Ceder, Y. Zhu, Revealing and rationalizing the rich polytypism of todorokite MnO_2, J. Am. Chem. Soc. 140 (22) (2018) 6961–6968.

[71] Y. Yuan, C. Zhan, K. He, H. Chen, W. Yao, S. Sharifi-Asl, B. Song, Z. Yang, A. Nie, X. Luo, H. Wang, S.M. Wood, K. Amine, M. Saiful Islam, J. Lu, The influence of large cations on the electrochemical properties of tunnel-structured metal oxides, Nat. Commun. 7 (2016) 13374.

[72] R. Yang, Y. Fan, R. Ye, Y. Tang, X. Cao, Z. Yin, Z. Zeng, MnO_2-Based materials for environmental applications, Adv. Math. 33 (9) (2021) 2004862.

[73] Y. Yuan, K. He, J. Lu, Structure–property interplay within microporous manganese dioxide tunnels for sustainable energy storage, Angew. Chem. Int. Ed. 63 (10) (2004) e202316055.

CORRECTED PROOF